Article

The Higgs Trilinear Coupling and the Scale of New Physics for the SM-Axion-Seesaw-Higgs Portal Inflation (SMASH) Model

C.R. Das [1,*] , Katri Huitu [2] and Timo J. Kärkkäinen [3]

1   Bogoliubov Laboratory of Theoretical Physics, Joint Institute for Nuclear Research – International Intergovernmental Organization, Joliot-Curie 6, 141980 Dubna, Moscow Region, Russia
2   Department of Physics and Helsinki Institute of Physics, University of Helsinki, P.O. Box 64, FI-00014 Helsinki, Finland
3   Laboratory of High Energy and Computational Physics, National Institute of Chemical Physics and Biophysics, Rävala 10, 10143 Tallinn, Estonia
*   Correspondence: das@theor.jinr.ru; Tel.: +7-962-915-9146

Abstract: In the extended scalar sector of the SMASH (Standard Model - Axion-Seesaw-Higgs portal inflation) framework, we conduct a phenomenological investigation of the observable effects. In a suitable region of the SMASH scalar parameter spaces, we solve the vacuum metastability problem and discuss the one-loop correction to the triple Higgs coupling, λ_{HHH}. The λ_{HHH} and SM Higgs quartic coupling λ_H corrections are found to be proportional to the threshold correction. A large λ_{HHH} correction ($\gtrsim 5\%$) implies vacuum instability in the model and thus limits the general class of theories that use threshold correction. We performed a full two-loop renormalization group analysis of the SMASH model. The SMASH framework has also been used to estimate the evolution of lepton asymmetry in the universe.

Keywords: Higgs portal inflation; beyond the standard model; SMASH; Higgs triple coupling; Higgs trilinear coupling

PACS: 12.60.-i; 14.80.Cp; 12.10.Kt; 11.10.Hi

1. Introduction

After the discovery of the Standard Model (SM) Higgs boson [1,2], every elementary particle of the SM has been confirmed to exist. Even though the past forty years have been a spectacular triumph for the SM, the mass of the Higgs boson ($m_H = 125.25 \pm 0.17$ GeV) [3] poses a serious problem for the SM [4]. It is well-known that the SM Higgs potential is metastable [5], as the sign of the quartic coupling, λ_H, turns negative at instability scale $\Lambda_{\text{IS}} \sim 10^{11}$ GeV. On the other hand, the SM is devoid of non-perturbative problems since the non-perturbative scale $\Lambda_{\text{NS}} \gg M_{Pl}$, where $M_{Pl} = 1.22 \times 10^{19}$ GeV is the Planck scale, but still there are studies on non-perturbative effects of the SM [6–10]. In the post-Planckian regime, effects of quantum gravity are expected to dominate, and the non-perturbative scale is therefore well beyond the validity region of the SM, unlike the instability scale. The largest uncertainties in SM vacuum stability are driven by top quark pole mass and the mass of the SM Higgs boson [11]. The current data are in significant tension with the stability hypothesis, making it more likely that the universe is in a false vacuum state [12–15]. The expected lifetime of vacuum decay to a true vacuum is extraordinarily long, and it is unlikely to affect the evolution of the universe [16,17]. However, it is unclear why the vacuum state entered into a false vacuum to begin with during the early universe. In this post-SM era, the emergence of vacuum stability problems (among many others) forces the particle theorists to expand the SM in such a way that the λ_H will stay positive during the run all the way up to the Planck scale.

It is possible that at or below the instability scale, heavy degrees of freedom originating from a theory beyond the SM start to alter the running of the SM parameters of renormalization group equations (RGE). It has been shown that incorporating the Type-I seesaw mechanism [18–28] will have a large destabilizing effect if the neutrino Yukawa couplings are large [29], and an insignificantly small effect if they are small. Thus, to solve the vacuum stability problem simultaneously with neutrino mass, a larger theory extension is required. Embedding the invisible axion model [30–32] together with the Type-I seesaw was considered in [33,34]. The axion appears as a phase of a complex singlet scalar field. This approach aims to solve the vacuum stability problem by proving that the universe is currently in a true vacuum. The scalar sector of such a theory may stabilize the vacuum with a threshold mechanism [35,36]. The effective SM Higgs coupling gains a positive correction $\delta \equiv \lambda_{H\sigma}^2/\lambda_\sigma$ at m_ρ, where $\lambda_{H\sigma}$ is the Higgs doublet-singlet portal coupling and λ_σ is the quartic coupling of the new scalar.

Corrections altering λ_H in such a model would also induce corrections to the triple Higgs coupling, $\lambda_{HHH}^{\text{tree}} = 3m_H^2/v$, where $v = 246.22$ GeV is the SM Higgs vacuum expectation value (VEV) [37–39]. The triple Higgs coupling is uniquely determined by the SM but is unmeasured. In fact, the Run 2 data from the Large Hadron Collider (LHC) has only been able to determine the upper limit of the coupling to be 12 times the SM prediction [3]. Therefore, future prospects of measuring a deviation of triple Higgs coupling by the high-luminosity upgrade of the LHC (HL-LHC) [40,41] or by a planned next-generation Future Circular Collider (FCC) [42–49] give us hints of the structure of the scalar sector of a beyond-the-SM theory. Previous work has shown that large corrections to triple Higgs coupling might originate from a theory with one extra Dirac neutrino [50,51], inverse seesaw model [52], two Higgs doublet model [38,39,53,54], one extra scalar singlet [37,55,56] or in the Type II seesaw model [57].

The complex singlet scalar, and consequently, the corresponding threshold mechanism, is embedded in a recent SMASH [58–60] theory, which utilizes it at $\lambda_{H\sigma} \sim -10^{-6}$ and $\lambda_\sigma \sim 10^{-10}$. The mechanism turns out to be dominant unless the new Yukawa couplings of SMASH are $\mathcal{O}(1)$. In addition to its simple scalar sector extension, SMASH includes electroweak singlet quarks Q and $\overline{Q}$ and three heavy right-handed Majorana neutrinos N_1, N_2 and N_3 to generate masses for neutrinos.

The structure of this paper is as follows: In Section 2, we summarize the SMASH model and cover the relevant details of its scalar sector. We also establish the connection between the threshold correction and the leading order λ_{HHH} correction. In Section 3, we discuss the methods, numerical details, RGE running, and our choice of benchmark points. Our results are presented in Section 4, where the viable parameter space is constrained by various current experimental limits. In SMASH, one can obtain at most $\sim$5% correction to λ_{HHH} while simultaneously stabilizing the vacuum. We give our short conclusions on Section 5.

2. Theory

The SMASH framework [58–60] expands the scalar sector of the SM by introducing a complex singlet field

$$\sigma = \frac{1}{\sqrt{2}}(v_\sigma + \rho)e^{iA/v_\sigma}, \tag{1}$$

where ρ and A (the axion) are real scalar fields, and $v_\sigma \gg v$ is the VEV of the complex singlet. The scalar potential of SMASH is then

$$
\begin{aligned}
V(H,\sigma) &= \lambda_H\left(H^\dagger H - \frac{v^2}{2}\right)^2 + \lambda_\sigma\left(|\sigma|^2 - \frac{v_\sigma^2}{2}\right)^2 \\
&\quad + 2\lambda_{H\sigma}\left(H^\dagger H - \frac{v^2}{2}\right)\left(|\sigma|^2 - \frac{v_\sigma^2}{2}\right).
\end{aligned}
\tag{2}
$$

Defining $\phi_1 = H$ and $\phi_2 = \sigma$, in basis (H, σ), the scalar mass matrix of this potential is

$$(M_{ij})_{\text{scalar}} = \frac{1}{2}\frac{\partial^2 V}{\partial \phi_i \partial \phi_j}\bigg|_{\substack{H = v/\sqrt{2}, \\ \sigma = v_\sigma/\sqrt{2}}} = \begin{pmatrix} 2\lambda_H v^2 & 2\lambda_{H\sigma} v v_\sigma \\ 2\lambda_{H\sigma} v v_\sigma & 2\lambda_\sigma v_\sigma^2 \end{pmatrix}, \tag{3}$$

which has eigenvalues

$$m_H^2 = v^2 \lambda_H + v_\sigma^2 \lambda_\sigma - \sqrt{v^4 \lambda_H^2 + 4v^2 v_\sigma^2 \lambda_{H\sigma}^2 - 2v^2 v_\sigma^2 \lambda_H \lambda_\sigma + v_\sigma^4 \lambda_\sigma^2}, \tag{4}$$

and

$$m_\rho^2 = v^2 \lambda_H + v_\sigma^2 \lambda_\sigma + \sqrt{v^4 \lambda_H^2 + 4v^2 v_\sigma^2 \lambda_{H\sigma}^2 - 2v^2 v_\sigma^2 \lambda_H \lambda_\sigma + v_\sigma^4 \lambda_\sigma^2}. \tag{5}$$

At the heavy singlet limit $\lambda_\sigma v_\sigma^2 \gg \lambda_H v^2$

$$m_H^2 = 2v^2 \left(\lambda_H - \frac{\lambda_{H\sigma}^2}{\lambda_\sigma} \right) + \mathcal{O}\left(\frac{v^2}{v_\sigma^2} \right), \tag{6}$$

and

$$m_\rho^2 = 2v_\sigma^2 \lambda_\sigma - 2v^2 \frac{\lambda_{H\sigma}^2}{\lambda_\sigma} + \mathcal{O}\left(\frac{v^4}{v_\sigma^2} \right). \tag{7}$$

Defining threshold correction $\delta \equiv \lambda_{H\sigma}^2/\lambda_\sigma$ in Equation (13),

$$m_H^2 \approx 2v^2(\lambda_H - \delta) \equiv 2v^2 \lambda_H^{\text{SM}}, \tag{8}$$

and

$$m_\rho^2 \approx 2v_\sigma^2 \lambda_\sigma - 2v^2 \delta. \tag{9}$$

The first term in the Equation (9) is the leading component.

The SMASH framework also includes a new quark-like field, Q, which has color but is an electro-weak singlet. It gains its mass via the Higgs mechanism, through a complex singlet σ. It arises from the Yukawa term

$$\mathcal{L}_Q^Y = Y_Q \overline{Q} \sigma Q \Rightarrow m_Q \approx \frac{Y_Q v_\sigma}{\sqrt{2}}. \tag{10}$$

We will show later that $Y_Q = \mathcal{O}(1)$ is forbidden by the vacuum stability requirement. The hypercharge of Q is chosen to be $q = -1/3$, even though $q = 2/3$ is possible. Our analysis is almost independent of the hypercharge assignment.

Threshold correction: Consider an energy scale below $m_\rho < \Lambda_{\text{IS}}$, where the heavy scalar ρ is integrated out. The low-energy Higgs potential should match the SM Higgs potential

$$V(H) = \lambda_H^{\text{SM}} \left(H^\dagger H - \frac{v^2}{2} \right)^2. \tag{11}$$

It turns out that the quartic coupling we measure has an additional term

$$\lambda_H^{\text{SM}} = \lambda_H - \frac{\lambda_{H\sigma}^2}{\lambda_\sigma}. \tag{12}$$

Since the SM Higgs quartic coupling will be approximately $\lambda_H(M_{Pl}) \approx -0.02$, the threshold correction

$$\delta \equiv \frac{\lambda_{H\sigma}^2}{\lambda_\sigma} \tag{13}$$

should have a minimum value close to $|\lambda_H(M_{Pl})|$ or slightly larger to push the high-energy counterpart λ_H to positive value all the way up to M_{Pl}. A too-large correction will,

however, increase λ_H too rapidly, exceeding the perturbativity limit $\sqrt{4\pi}$. We demonstrate the conditions for δ in Section 4. Similar to λ_H, the SM Higgs quadratic parameter μ_H gains a threshold correction

$$\left(\mu_H^{\text{SM}}\right)^2 = \mu_H^2 - \frac{\lambda_{H\sigma}}{\lambda_\sigma}\mu_\sigma^2. \tag{14}$$

In the literature [35,36], there are two possible ways of implementing this threshold mechanism. One may start by solving the SM RGE's up to m_ρ, where the new singlet effects kick in, and the quadratic and quartic couplings gain sudden increments. Continuation of RGE analysis to even higher scales then requires utilizing the new RGE's up to the Planck scale.

Another approach is to only solve the new RGEs on the SM scale while ignoring the low-scale SM RGEs entirely. We will use the former approach.

One-loop correction to triple Higgs coupling: The portal term of the Higgs potential contains the trilinear couplings for $HH\rho$ and $H\rho\rho$ vertices. The vertex factors for $HH\rho$ and $H\rho\rho$ vertices are introduced in Figure 1. The one-loop diagrams contributing to SM triple Higgs coupling are in Figure 2. We denote the SM tree-level triple Higgs coupling as λ_{HHH}. The correction is gained by adding all the triangle diagrams (taking into account the symmetry factors)

$$
\begin{aligned}
\Delta\lambda_{HHH} &= \left(2^2 \cdot \lambda_{HHH}\lambda_{H\sigma}^2 v_\sigma^2 I(m_H, m_H, m_\rho; p, q) + 2\,\text{permutations}\right) \\
&\quad + \left(2^3 \cdot \lambda_{H\sigma}^3 v v_\sigma^2 I(m_H, m_\rho, m_\rho; p, q) + 2\,\text{permutations}\right) \\
&\quad + 2^3 \cdot \lambda_{H\sigma}^3 v^3 I(m_\rho, m_\rho, m_\rho; p, q).
\end{aligned}
\tag{15}
$$

Here, p and q are the external momenta and the loop integral is defined as

$$I(m_A, m_B, m_C; p, q) =$$

$$\int \frac{d^4k}{(2\pi)^4} \frac{1}{(k^2 - m_A^2)((k-p)^2 - m_B^2)((k+q)^2 - m_C^2)}. \tag{16}$$

The contribution from diagram Figure 3 is subleading, since it is proportional to $\lambda_{H\sigma}^2 v \Rightarrow \delta\lambda_\sigma v \ll \lambda_{HHH}$.
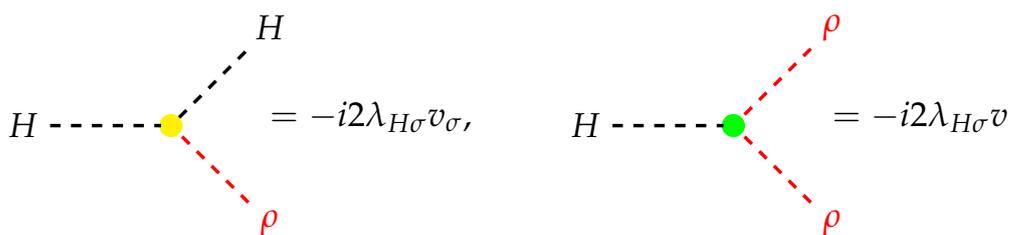
Figure 1. Vertex factors on trilinear vertices involving the SM Higgs boson as well as a real singlet ρ. They can be derived from Equation (2). We denote ρ and its propagator by red color.
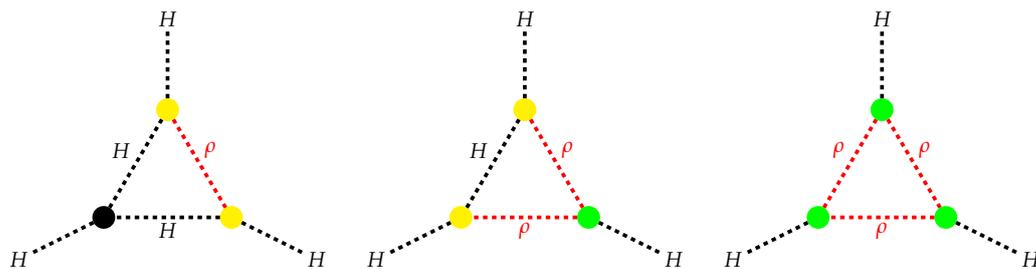
Figure 2. One-loop corrections to SM triple Higgs coupling induced by the existence of an extra scalar singlet. In Equation (15), the correction $\Delta\lambda_{HHH}$ is derived.
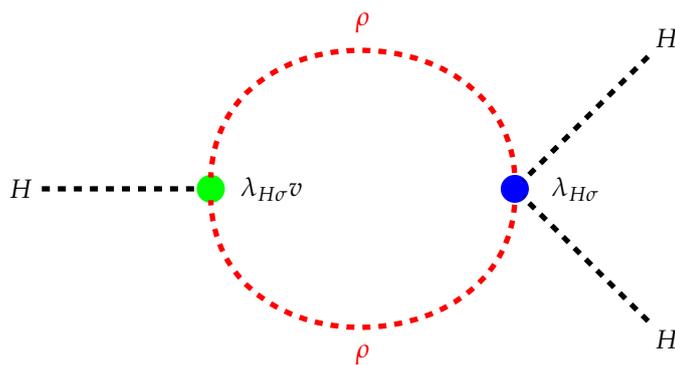
Figure 3. One-loop SM triple Higgs coupling correction diagram with a cubic vertex and a quartic vertex.

The process $H^* \to HH$ is disallowed for on-shell external momenta, so at least one of them must be off-shell. Specifically, the momentum-dependent correction to the triple coupling at the tree-level is an effective coupling that enters the specific process with one off-shell Higgs decaying into two real Higgses. Note that the correction is dependent on the Higgs off-shell momentum $q \equiv q^*$, which we assume to be at $\mathcal{O}(1)$ TeV at the LHC and HL-LHC. The first diagram is dominant due to the heaviness of the ρ scalar. Therefore, we may ignore the subleading contributions of diagrams involving two or more ρ propagators. We integrate out the heavy scalar, causing the finite integral in Equation (16) to be logarithmically divergent. We calculate the finite part of it using dimensional regularization and obtain

$$
\begin{aligned}
\Delta\lambda_{HHH} &= -4\lambda_{HHH}\left(\frac{v_\sigma}{m_\rho}\right)^2\left(\frac{\lambda_{H\sigma}^2}{16\pi^2}\right)\left(2 + \ln\frac{\mu^2}{m_H^2} - z\ln\frac{z+1}{z-1}\right) \\
&\simeq -2\lambda_{HHH}\left(\frac{\delta}{16\pi^2}\right)\left(2 + \ln\frac{\mu^2}{m_H^2} - z\ln\frac{z+1}{z-1}\right),
\end{aligned}
\tag{17}
$$

where $z \equiv \sqrt{1 + (4m_H^2/q^2)}$ and $\mu = m_\rho$ is the regularization scale[1]. We have used the modified minimal subtraction scheme ($\overline{\text{MS}}$), where the terms $\ln 4\pi$ and Euler–Mascheroni constant $\gamma_E \approx 0.57722$ emerging in the calculation are absorbed to the regularization scale μ. For calculations, we use the value $q^* = 1$ TeV. It is especially interesting to see that at the leading order, the triple Higgs coupling correction is proportional to the threshold corrections. This intimate connection forbids a too-large correction. In fact, the bound from vacuum stability turns out to constrain the triple Higgs coupling correction to $\lesssim 5\%$, as we shall see in Section 4. Consequently, if LHC or HL-LHC manages to measure a correction to λ_{HHH}, this will rule out theories that utilize exclusively threshold correction mechanisms as a viable solution to the vacuum stability problem. Indeed, there are alternate ways to produce large $\Delta\lambda_{HHH}$ without expanding the scalar sector [50,52].

It should be noted that loop corrections contributing to the final to-be-observed value are included in the SM. Indeed, experiments are measuring $\lambda_{HHH}^{\text{SM}} = \lambda_{HHH}^{\text{SM(tree)}} + \lambda_{HHH}^{\text{SM(1-loop)}}(q^*) + \dots$, where the SM one-loop correction depends on the Higgs off-shell momentum. At the $\mathcal{O}(1)$ TeV scale we are considering, the SM 1-loop correction amounts to approximately -7% [50].

Light neutrino masses: The neutrino sector of SMASH is able to generate correct neutrino masses and observe the baryon asymmetry of the universe with suitable benchmarks. The relevant Yukawa terms for neutrinos in the model are

$$
\mathcal{L}_\nu^Y = -\frac{1}{2}Y_n^{ij}\sigma N_i N_j - Y_\nu^{ij}L_i\varepsilon H N_j.
\tag{18}
$$

We take a simplified approach: Dirac and Majorana Yukawa matrices (Y_ν and Y_n, respectively) are assumed to be diagonal.

$$Y_\nu = \begin{pmatrix} y_1 & 0 & 0 \\ 0 & y_2 & 0 \\ 0 & 0 & y_3 \end{pmatrix}, \quad Y_n = \begin{pmatrix} Y_1 & 0 & 0 \\ 0 & Y_2 & 0 \\ 0 & 0 & Y_3 \end{pmatrix}. \tag{19}$$

To generate baryonic asymmetry in the universe, SMASH utilizes the thermal leptogenesis scenario [61], which generates lepton asymmetry in the early universe and leads to baryon asymmetry. In the scenario, heavy neutrinos require a sufficient mass hierarchy [62,63] and one or more Yukawa couplings must have complex CP phase factors. We assume the CP phases are $\mathcal{O}(1)$ radians to near-maximize the CP asymmetry [64–66]

$$\varepsilon_{\mathrm{CP}} = \frac{\Gamma(N_1 \to H + \ell_L) - \Gamma(N_1 \to H^\dagger + \ell_L^\dagger)}{\Gamma(N_1 \to H + \ell_L) + \Gamma(N_1 \to H^\dagger + \ell_L^\dagger)} \lesssim \frac{3M_1 m_3}{16\pi v^2}. \tag{20}$$

If the CP violation is maximal, the largest value is obtained. To produce matter–antimatter asymmetry in the universe, a large asymmetry is required. Following [58], we set the heavy neutrino mass hierarchy at $M_3 = M_2 = 3M_1$, corresponding to $Y_3 = Y_2 = 3Y_1$. These choices give the full 6×6 neutrino mass matrix

$$M_\nu = \begin{pmatrix} \mathbf{0}_{3\times3} & m_D \\ m_D^T & M_M \end{pmatrix}, \tag{21}$$

which is in block form, and contains two free parameters: v_σ and Y_1. Here, $m_D = Y_\nu v/\sqrt{2}$ is the Dirac mass term and $M_M = Y_n v_\sigma/\sqrt{2}$ is the Majorana mass term. Light neutrino masses are then generated via the well-known Type I seesaw mechanism [18–28], by block diagonalizing the full neutrino mass matrix M_ν.

It is possible to obtain light neutrino masses consistent with experimental constraints from atmospheric and solar mass splittings Δm_{32}^2 and Δm_{21}^2 [67] and cosmological constraint $m_1 + m_2 + m_3 < 0.12$ eV [68–73] (corresponding to $m_1 \lesssim 0.03$ (0.055) eV with normal (inverse) neutrino mass ordering, from Equations (10)–(12) and Figure 1 of [74] for upper bound), assuming the standard ΛCDM cosmological model [74–78]. However, the total mass $m_1 + m_2 + m_3$ should not be less than 0.06 (0.10) eV for normal (inverse) hierarchy as per Equation (13) of [74].

The light neutrino mass matrix is

$$m_\nu = -\frac{v^2}{\sqrt{2}v_\sigma} Y_\nu Y_n^{-1} Y_\nu^T. \tag{22}$$

After removing the irrelevant sign via field redefinition,

$$\begin{aligned} m_\nu &= C \begin{pmatrix} y_1^2/Y_1 & 0 & 0 \\ 0 & y_2^2/Y_2 & 0 \\ 0 & 0 & y_3^2/Y_3 \end{pmatrix} \\ &= \begin{pmatrix} m_1 & 0 & 0 \\ 0 & \sqrt{m_1^2 + \Delta m_{31}^2} & 0 \\ 0 & 0 & \sqrt{m_1^2 + \Delta m_{21}^2 + \Delta m_{32}^2} \end{pmatrix}, \end{aligned} \tag{23}$$

where we have denoted $C = v^2/(\sqrt{2}v_\sigma)$ and assumed normal mass ordering $m_1 < m_2 < m_3$. This gives the neutrino masses $m_i = C y_i^2/Y_i$. We do not know the absolute masses, but the mass squared differences have been measured by various neutrino oscillation experiments [67,79]. Nevertheless, their values provide two constraints, leaving three free parameters. However,

the heavy neutrino Yukawa couplings Y_i must be no larger than $\mathcal{O}(10^{-3})$ to avoid vacuum instability [59].

In addition, an order-of-magnitude estimate of the generated matter–antimatter asymmetry (baryon-to-photon ratio) is directly proportional to the CP asymmetry

$$\eta \equiv \frac{n_B}{n_\gamma} = \mathcal{O}\left(10^{-2}\right)\varepsilon_{\text{CP}}\kappa, \tag{24}$$

where $\kappa \sim 0.01$–0.1 is an efficiency factor. We arrive at

$$\eta = \mathcal{O}\left(10^{-10}\right) \times \frac{v_\sigma}{10^8 \text{ GeV}} \times \frac{Y_1}{10^{-2}} \times \frac{\kappa}{0.1}, \tag{25}$$

which, in principle, can be consistent with the observed η. To achieve successful resonance leptogenesis, v_σ should be between 10^{10} and 10^{12} GeV (Table 1). We will provide suitable benchmark points in the next section. The estimation of lepton asymmetry, which is one of the crucial implications of SMASH as the framework claims to solve the matter-asymmetry issue since the scenario only consists of the decay and inverse decay of N_2 or N_3 to N_1. The leptogenesis evolution for the benchmark values shown in Table 2 is in Figure 4.

Table 1. Used benchmark points **(BP)** in our analysis. Note that we assume specific texture to right-handed neutrino Yukawa matrix Y_n.

Benchmarks	BP1	BP2	BP3
y_1	1.118×10^{-7}	1.312×10^{-5}	9.610×10^{-6}
y_2	7.754×10^{-4}	5.347×10^{-4}	1.893×10^{-3}
y_3	1.878×10^{-3}	1.309×10^{-3}	4.582×10^{-3}
Y_1	9.947×10^{-3}	9.614×10^{-3}	8.423×10^{-3}
Y_Q	10^{-3}	10^{-3}	10^{-3}
v_σ (GeV)	10^{11}	5×10^{10}	7×10^{11}
λ_σ	7.2×10^{-9}	4.48×10^{-7}	2.48×10^{-7}
$\lambda_{H\sigma}$	-3×10^{-5}	-2.25×10^{-4}	-1.67×10^{-4}

Table 2. The computed values of neutrino masses for normal hierarchy ($m_1 < m_2 < m_3$), the sum of light neutrino masses, and light neutrino mass squared differences. These neutrino masses are within experimental limits [67–73,79]. meV is Milli(10^{-3}) (symbol m) eV.

Benchmarks	BP1	BP2	BP3	Experimental Values
m_1 (meV)	5.39×10^{-7}	0.015	6.71×10^{-4}	$\lesssim 55$ (Equations (10) & (11) and Figure 1 of [74]
m_2 (meV)	8.64	8.50	8.68	with mass bound from [68])
m_3 (meV)	50.67	50.93	50.88	$\lesssim 60$ (Equation (12) and Figure 1 of [74] with mass bound from [68])
$m_1 + m_2 + m_3$ (meV)	59.30	59.45	59.57	< 120 [68,70] but, $\gtrsim 60$ (Equation (13) of [74])
Δm_{21}^2 (10^{-5} eV^2)	7.46	7.22	7.54	6.79–8.0 [67,79]
$|\Delta m_{32}^2|$ (10^{-3} eV^2)	2.57	2.59	2.59	2.412–2.625 [67,79]
M_1 (GeV)	7.03×10^8	3.40×10^8	4.17×10^9	Unknown
M_2, M_3 (GeV)	2.11×10^9	1.02×10^9	1.25×10^{10}	
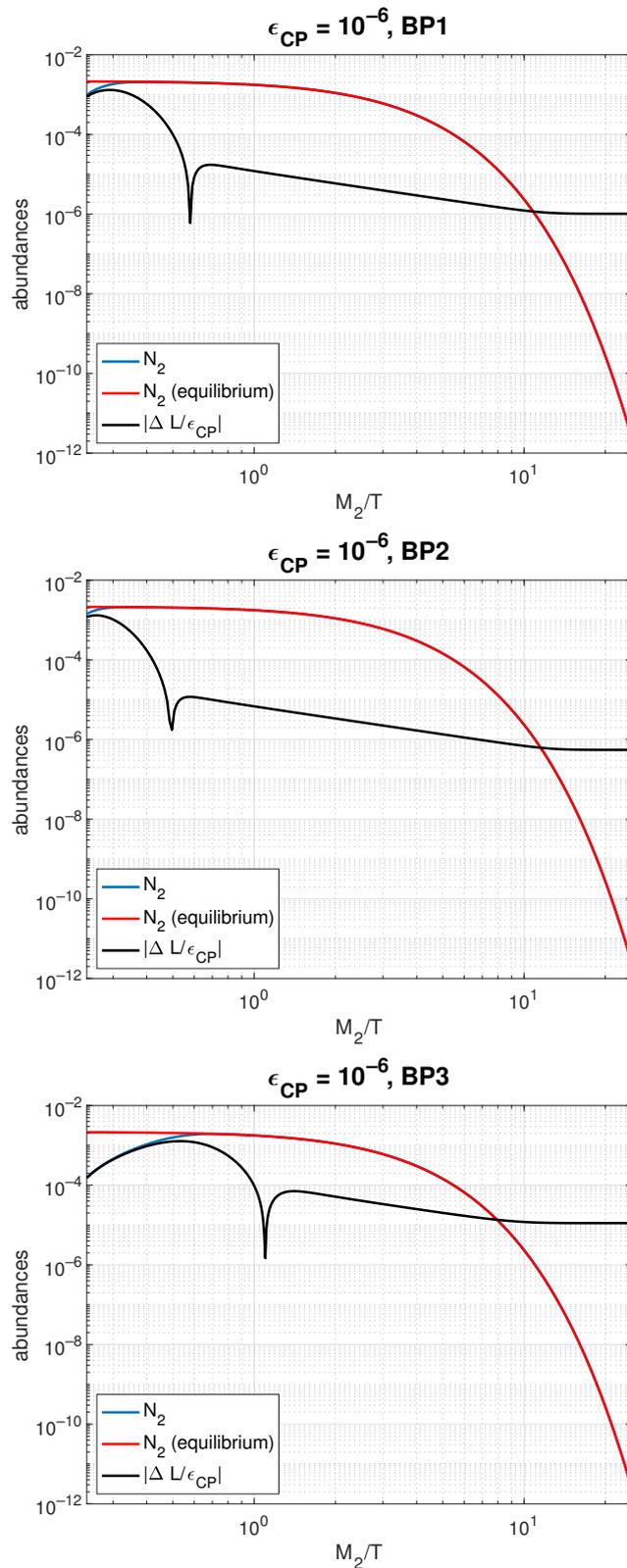
Figure 4. The evolution of the "abundance" of N_2 in blue, the "abundance" of N_2 in thermal equilibrium in red, and the lepton asymmetry generated by the CP violating decays and inverse decays of N_2 divided by the CP asymmetry parameter ε_{CP} in black. T is the temperature of the universe in GeV, as well as the mass of heavy neutrinos M_2 in GeV. ΔL is the number of changes in lepton number over entropy density s.

We will investigate the influence of N_1, N_2, and N_3 oscillations (i.e., right-handed neutrino oscillations) on leptogenesis evolutions, predict baryon-to-photon ratios for different set masses of light active left-handed neutrinos, and evaluate a more precise value of κ by solving complicated Boltzmann equations in the future course of analysis in the SMASH framework.

3. Methods

We generate the suitable benchmark points demonstrating different physics aspects of the model in the neutrino sector by fitting in the known neutrino mass squared differences Δm_{ij}^2, assuming normal mass ordering ($m_1 < m_2 < m_3$). This leaves three free neutrino parameters, the values of which we generate by logarithmically distributed random sampling. These are the candidates for benchmark points. We then require that the candidate points be consistent with the bounds for the sum of light neutrino masses [68–78]. The next step is to choose suitable values for other unknown parameters, using the stability of the vacuum as a requirement.

The authors of [58] have generated the corrections to the two-loop β functions of SMASH. We solve numerically the full two-loop 14 coupled renormalization group differential equations with SMASH corrections with respect to Yukawa ($Y_u, Y_d, Y_e, Y_\nu, Y_n, Y_Q$), gauge ($g_1, g_2, g_3$) and scalar couplings ($\mu_H^2, \mu_S^2, \lambda_H, \lambda_\sigma, \lambda_{H\sigma}$), ignoring the light SM degrees of freedom, from M_Z to Planck scale. We assume Yukawa matrices are on a diagonal basis, with the exception of Y_ν. We use the $\overline{\text{MS}}$ scheme for the running of the RGE's. Since the top quark $\overline{\text{MS}}$ mass is different from its pole mass, the difference is taken into account via the relation [80]

$$m_t^{\text{pole}} \approx m_t^{\overline{\text{MS}}}\left(1 + 0.4244\alpha_3 + 0.8345\alpha_3^2 + 2.375\alpha_3^3 + 8.615\alpha_3^4\right), \tag{26}$$

where $\alpha_3 \equiv g_3^2/4\pi \approx 0.1085$ at $\mu = m_Z$. We define the Higgs quadratic coupling as $\mu_H = m_H/\sqrt{2}$ and quartic coupling as $\lambda_H = m_H^2/2v^2$.

We use MATLAB R2019's `ode45`-solver. See Table 1 for the used SMASH benchmark points and Table 3 for our SM input [3]. Our scale convention is $t \equiv \log_{10}\mu/\text{GeV}$.

Table 3. Used SM inputs in our analysis, at $\mu = m_Z = 91.18$ GeV, with the exception of top mass, which is evaluated at $\mu = m_t$. Masses and vacuum expectation values are in GeV units [3].

Parameter	$m_t^{\overline{\text{MS}}}(m_t)$	m_b	m_H	m_τ	v	g_1	g_2	g_3	λ_H
Value	164.0	4.18	125.25	1.777	246.22	0.357	0.652	1.221	0.126

In some papers, the running of SM parameters ($Y^t, Y^b, Y^\tau, g_1, g_2, g_3, \mu_H^2, \lambda_H$) obeys the SM RGE's without corrections from a more effective theory until some intermediate scale Λ_{BSM} [35], after which the SM parameters gain threshold correction (where it is relevant) and the running of all SM parameters follows the new RGE's from that point onwards. We choose to utilize this approach while acknowledging an alternative approach, where the threshold correction is applied at the beginning ($\mu = m_Z$) [36], and both approaches give almost the same results. As previously stated, SM Higgs quadratic and quartic couplings will gain the threshold correction.

Our aim is to find suitable benchmark points, which:

- Allow the quartic and Yukawa couplings of the theory to remain positive and perturbative up to the Planck scale;
- Utilize a threshold correction mechanism to λ_H via $\delta \simeq 0.1$;
- Avoid the overproduction of dark radiation via the cosmic axion background (requiring $\lambda_{H\sigma} < 0$);
- Produce a significant contribution matter–antimatter asymmetry via leptogenesis (requiring hierarchy between the heavy neutrinos);
- Produce a ~5% correction to triple Higgs coupling λ_{HHH}.

4. Results

Stability of vacuum: We have plotted how the running of the SM quartic coupling, λ_H changes with each benchmark point in Figure 5. Note that all the threshold corrections are utilized well before the SM instability scale Λ_{IS}. One can choose $v_\sigma > \Lambda_{\text{IS}}$ if $m_\rho < \Lambda_{\text{IS}}$ is ensured. This is the case with **BP3**.
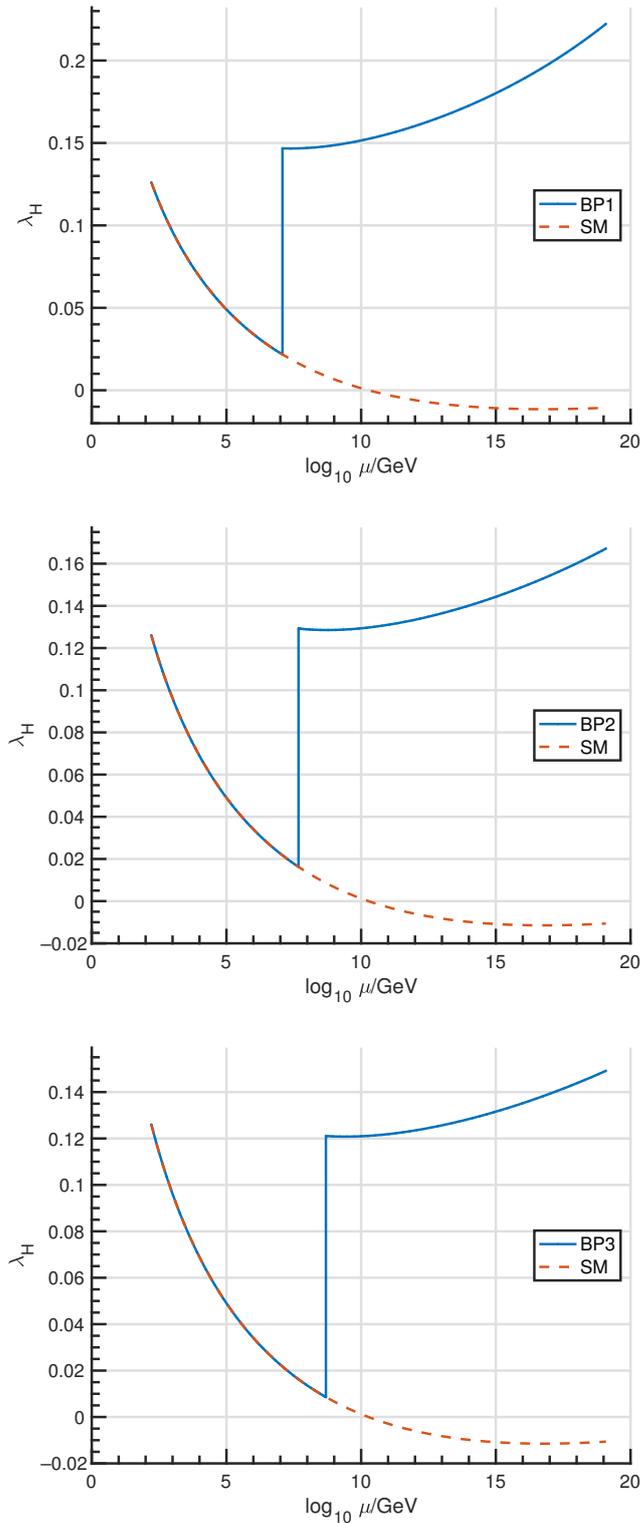
Figure 5. Running of SM Higgs quartic coupling in Standard Model (dashed line) and in SMASH with benchmark points **BP1**–**BP3** (solid line). Threshold correction is utilized at m_ρ.

We numerically scanned over the parameter space $m_t^{\text{pole}} \in [164, 182]$ GeV and $m_H \in [110, 140]$ GeV to analyze vacuum stability in three different benchmark points **BP1**–**BP3**. Our results for the chosen benchmarks are in Figure 6, where the SM best fit is denoted by a red star. Clearly, the electroweak vacuum is stable with our benchmark points, and it is assigned to $m_t^{\text{pole}} \simeq 172.69 \pm 0.3$ GeV and $m_H \simeq 125.25 \pm 0.17$ GeV [3]. For every case, we investigated the running of the quartic couplings of the scalar potential. We used the following stability conditions

$$\lambda_H(\mu) > 0, \quad \lambda_\sigma(\mu) > 0, \quad \lambda_H(\mu)\lambda_\sigma(\mu) > \lambda_{H\sigma}(\mu)^2, \tag{27}$$

and for $\lambda_{H\sigma} < 0$ [35]

$$-\lambda_{H\sigma}(\mu) < \sqrt{\lambda_H(\mu)\lambda_\sigma(\mu)}. \tag{28}$$

If one or more conditions are not met on the scale $\mu \in [m_Z, M_{Pl}]$, we denote this point as unstable. If any of the quartic couplings rises above $\sqrt{4\pi}$, we denote this point non-perturbative.
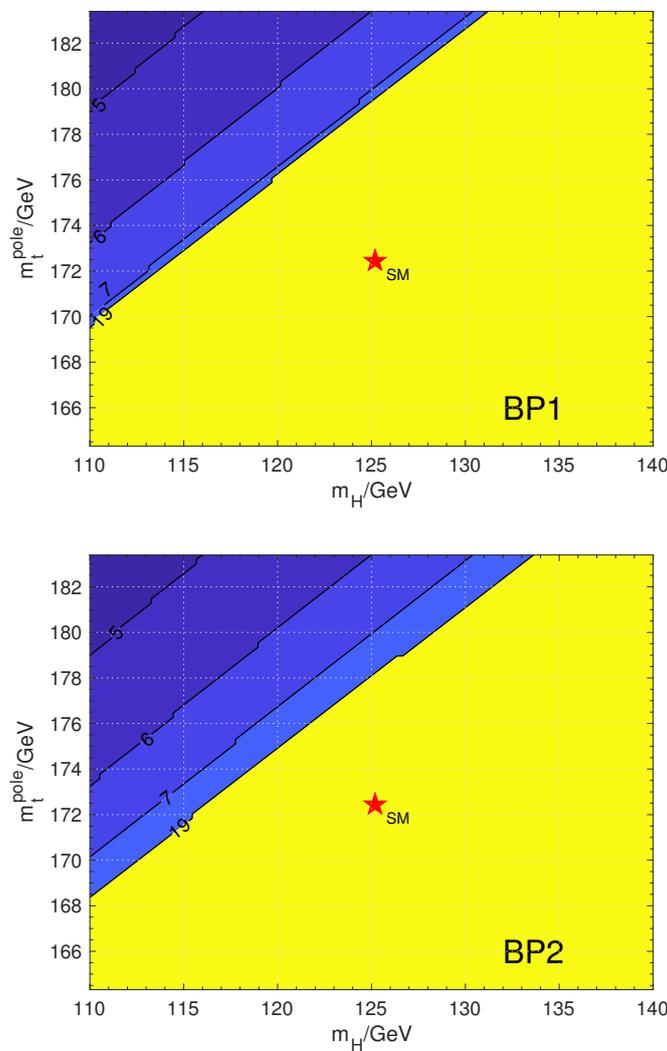
Figure 6. *Cont.*
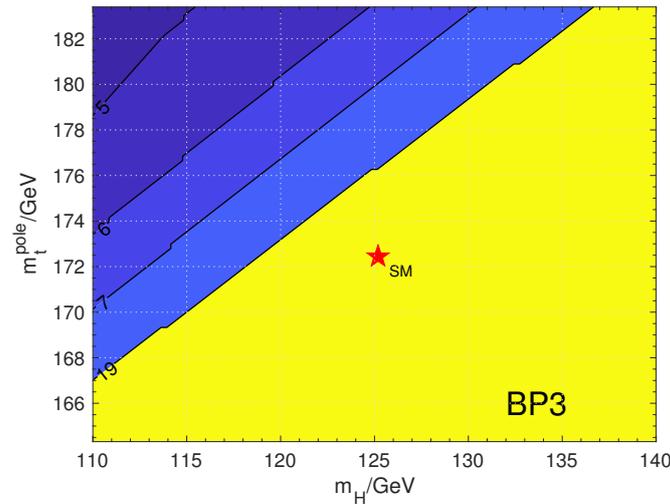
Figure 6. Vacuum stability of SMASH in (m_H, m_t^{pole}) plane with benchmark points **BP1**–**BP3**. The red star corresponds to the SM best-fit value. The height and width of the star correspond to the present uncertainties. The vacuum is stable in the yellow region. The contour numbers n correspond to the vacuum instability scale 10^n GeV.

We chose the new scalar parameters in such a way that the threshold correction is large but allowed, $0.1 < \delta < \lambda_H$. This changes the behavior of the coupling's running so that after the correction, the λ_H *increases* in energy instead of decreasing, the opposite of the coupling's running in a pure SM scenario. A too-large threshold correction will have an undesired effect, lowering the non-perturbative scale to energies lower than the Planck scale. These effects are visualized in Figure 7, where for each benchmark point kept λ_σ at its designated value in Table 1. Instead, we let the portal coupling, $\lambda_{H\sigma}$, vary between 0 and $\sqrt{0.6\lambda_\sigma}$. This demonstrates the small range of viable parameters space.
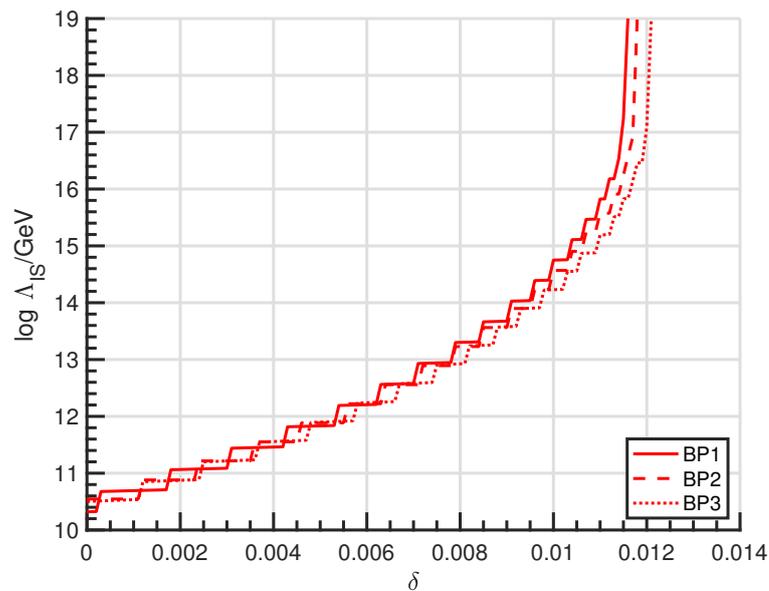
Figure 7. *Cont.*
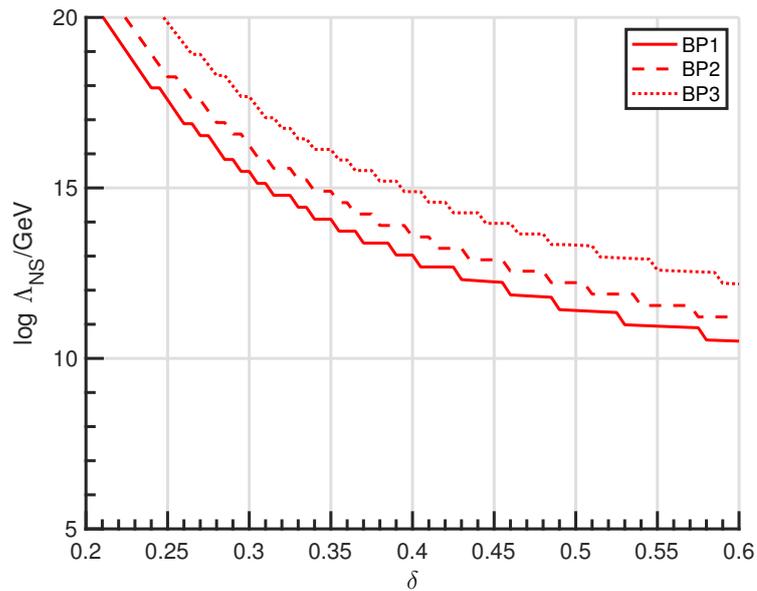
Figure 7. The rise of the instability scale (**above**) and the fall of the non-perturbative scale (**below**) as a function of threshold correction δ, for **BP1**–**BP3**.

We have also investigated the significance of v_σ on the bounds of threshold correction δ. A choice of δ is available as long as $v_\sigma \lesssim 2 \times 10^{13}$ GeV. This can be seen clearly from Figure 8. Given a fixed δ, the result is independent of $\lambda_{H\sigma}$ and λ_σ. The lower and higher bound for δ increases as a function of v_σ. Instability bound increases, since the needed vacuum-stabilizing threshold effect increases as one approaches the SM instability scale Λ_{IS}. At $v_\sigma \gtrsim 2 \times 10^{13}$ GeV, the $m_\rho > \Lambda_{IS}$, so the quartic coupling λ_H will turn negative before threshold correction is utilized. On the other hand, the non-perturbative scale increases, since, as the cutoff point m_ρ increases, the quartic coupling λ_H decreases and correspondingly, the largest possible threshold correction increases.
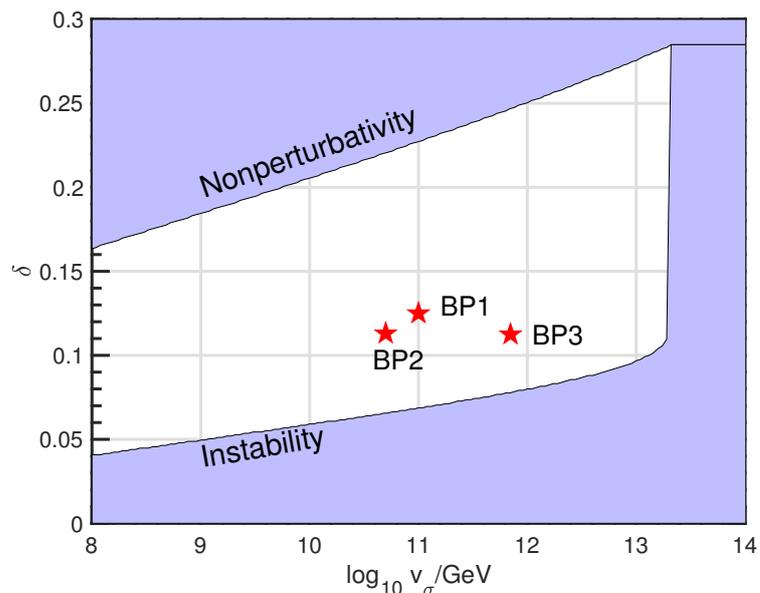
Figure 8. The available parameter space is consistent with a stable vacuum in (v_σ, δ) space. λ_σ is fixed, while $\lambda_{H\sigma}$ is determined by Equation (13) and m_ρ by Equation (9). We have denoted our benchmark points with a red star.

Our next scan was over the new quartic couplings, $\log_{10}(-\lambda_{H\sigma}) \in [-7,0]$ and $\log_{10}\lambda_\sigma \in [-10,0]$. The scalar potential is stable and the couplings remain perturbative at only a narrow band, where $\delta \sim 0.01$–0.1, see Figure 9. If one considers small δ, the SM Higgs quartic coupling will decrease to near zero at $\mu = M_{Pl}$. This corresponds to a region near the left side of the stability band. In contrast, we chose our benchmarks with large δ, placing it near the right side of the stability band, corresponding to the large value of λ_H at $\mu = M_{Pl}$. This was a deliberate choice to maximize the correction to λ_{HHH}.
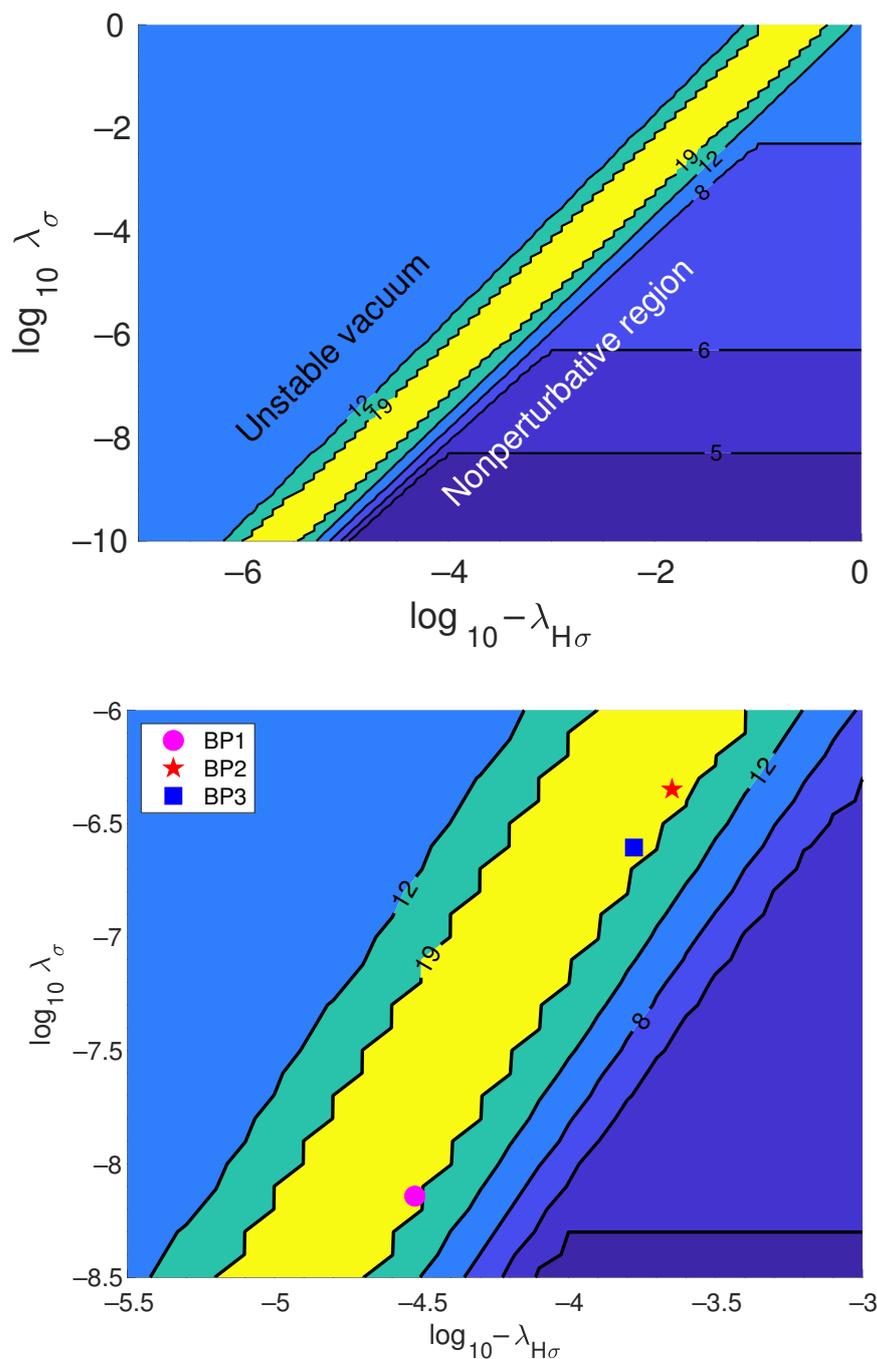
Figure 9. (**Above**): Different regions in the logarithmic $(-\lambda_{H\sigma}, \lambda_\sigma)$ plane. The contour numbers n above the yellow band correspond to the vacuum instability scale 10^n GeV. Below the yellow band, the contour numbers m correspond to the non-perturbative scale 10^m GeV. The color coding is interpreted as in Figure 6. For non-perturbative scale calculations, we used **BP1**. (**Below**): Zoomed-in detail of the figure above, showing in addition our chosen benchmarks.

In addition, we have scanned the Dirac neutrino and new quark-like particle Yukawa couplings (y_1 and Y_Q, respectively) over $y_1 \in [0, 2]$ and $Y_Q \in [0, 0.04]$, keeping y_2 and y_3 small, real[2] and positive but non-zero. See Figure 10 for details corresponding to each benchmark point. There, we point to an area producing a stable vacuum. The Dirac neutrino Yukawa couplings may have a maximum value of $\mathcal{O}(1)$, but a more stringent constraint is found for Y_Q. It should be noted that even though, from the vacuum instability point of view, $Y_Q^{\max} < y_1^{\max}$, this does not imply $Y_Q < y_1$, since both are in principle free parameters. See Table 2 for computed values for neutrino masses for normal hierarchy ($m_1 < m_2 < m_3$) corresponding to each benchmark. Note that all **BP1**–**BP3** produce a value of baryon-to-photon ratio comparable to experimental values and a mass of axion consistent with axion dark matter scenario, because it requires axion decay constant $f_A \equiv v_\sigma$ to be $\mathcal{O}(10^{11})$ GeV [30–32].
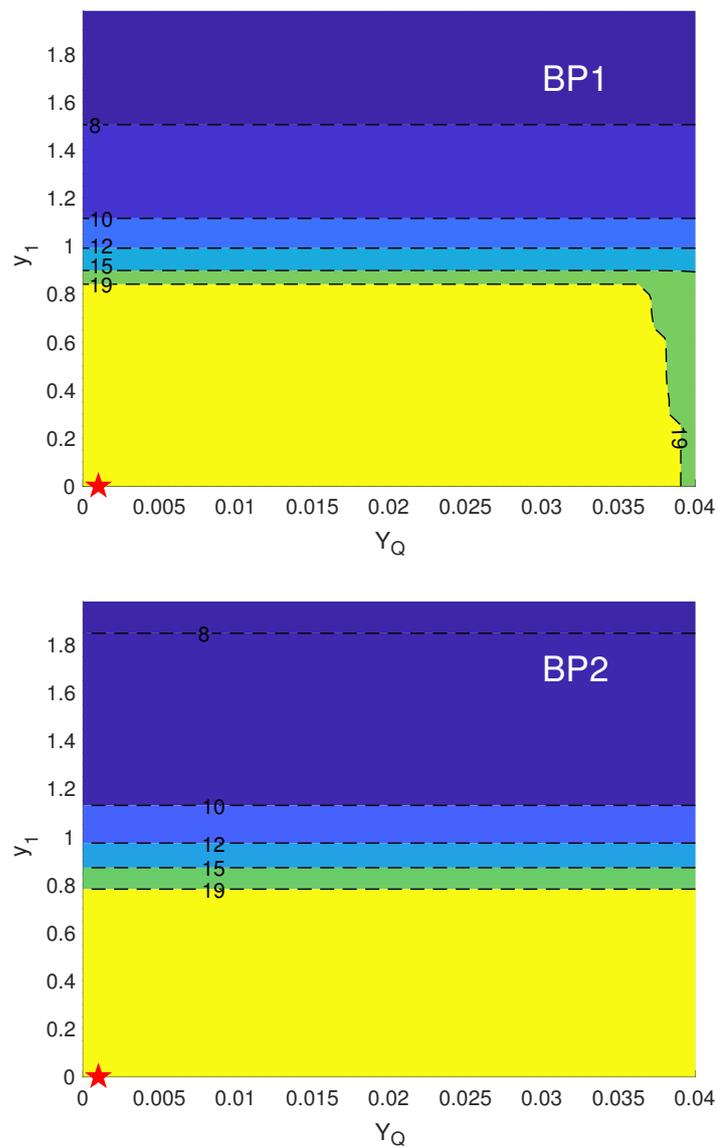
Figure 10. *Cont.*
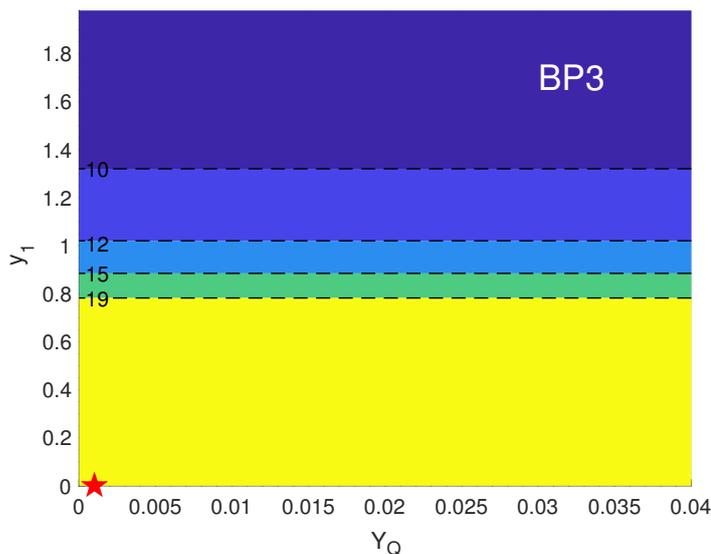
Figure 10. Vacuum instability scales in (Y_Q, y_1) plane in benchmark points **BP1**–**BP3**. The red star corresponds to the chosen benchmark point value. The color coding and the contour numbers are interpreted as in Figure 6.

In Figure 4, we show the evolution of N_2 or N_3 abundance, as well as the lepton asymmetry generated by the CP violating decays and inverse decays of N_2 or N_3, divided by the CP asymmetry parameter ε_{CP} as per [62]. The resulting lepton asymmetry is translated to baryon asymmetry via the sphaleron process with a c_s fraction. We have also shown the N_2 or N_3 abundance in thermal equilibrium. The number density n of particles decreases in an expanding universe if there are now particle number-changing interactions. However, the ratio of number density n to entropy density s, that is, "abundance" $= n/s$, is constant. Changing "abundance" during the early universe thus indicates particle interactions, or in our case, N_2 or N_3 decays and inverse decays. A corresponding mass hierarchy for right-handed neutrinos implies an upper bound of $\varepsilon_{CP} \sim 10^{-5}$ to 10^{-6} [63,81].

Correction to SM triple Higgs coupling: According to PDG [3], the largest possible experimental value for λ_{HHH} is 12 times the SM prediction[3], from Run 2 data for the $b\bar{b}\gamma\gamma$ channel alone. The real singlet scalar ρ mixes with the SM Higgs, providing a one-loop correction to SM triple Higgs coupling λ_{HHH}. We scanned the parameter space with $\log_{10}(-\lambda_{H\sigma}) \in [-7, 0]$ and $\log_{10} \lambda_\sigma \in [-10, 0]$. At each point, we calculated the correction to λ_{HHH}. See Figure 11 for details. We identified a section of parameter space excluded by triple Higgs coupling searches from LHC run 2 and determined the area sensitive to future experiments, namely, HL-LHC and FCC-hh. We assume HL-LHC uses 14 TeV center-of-mass energy and integrated luminosity $\mathcal{L} = 3\,\text{ab}^{-1}$, for FCC-hh we assume center-of-mass energy 100 TeV and integrated luminosity $\mathcal{L} = 3\,ab^{-1}$. The relative correction in Table 4 is calculated with respect to the SM tree-level prediction. We chose our benchmark points in a way that their correction to triple Higgs coupling will be borderline observable at FCC-hh [82], that is, the correction will be ∼5%. Thus, η in BP3 for a factor of 10 larger is necessary for stable vacuum and FCC-hh better detection shown in Figure 11. Future FCC-hh accelerator is sensitive to ∼5% deviation of the Standard Model prediction. This is demonstrated by the benchmark points we have chosen. Although the model's stable region allows for even smaller deviations, part of the region is still accessible by FCC-hh.
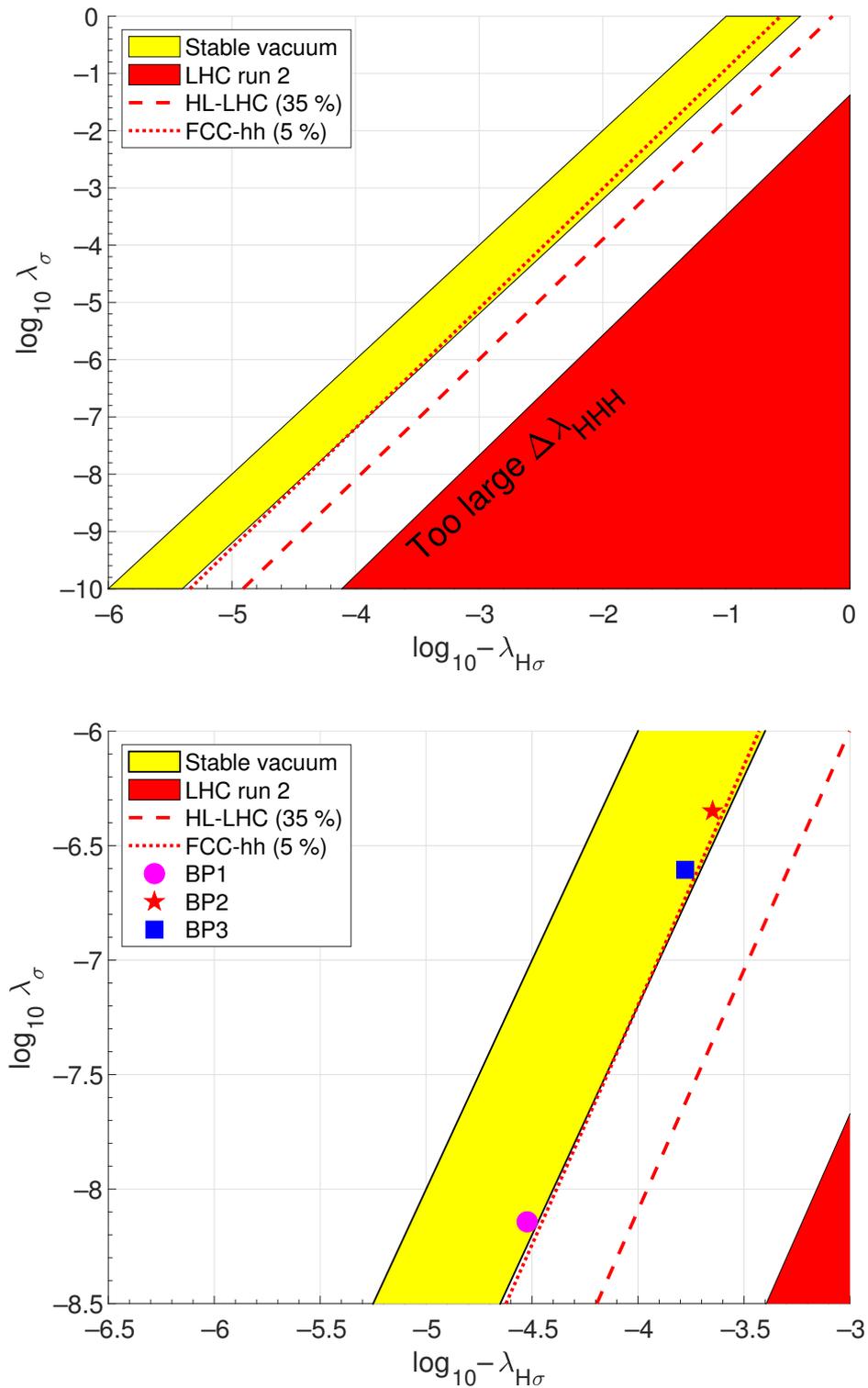
Figure 11. (Above): Different regions in the logarithmic $(-\lambda_{H\sigma}, \lambda_\sigma)$ plane. The yellow band corresponds to a stable vacuum configuration. The red area is excluded from the second run of the Large Hadron Collider since the triple Higgs coupling corrections to SMASH would be too large. The dashed line corresponds to the expected sensitivity of the high-luminosity LHC, and the dotted line to the expected sensitivity of the Future Circular Collider in hadronic collision mode. **(Below)**: Zoomed-in detail of the figure above, showing in addition our chosen benchmarks.

Table 4. The computed values of threshold correction δ, BSM scalar masses m_A and m_ρ, baryon-to-photon ratio η, quartic self-couplings at M_{Pl}, correction to the triple Higgs coupling $\Delta\lambda_{HHH}$ compared to the SM prediction.

Benchmarks	BP1	BP2	BP3	Experimental Values
$\delta(\mu = m_\rho)$	0.125	0.113	0.113	None
m_A (eV)	5.7×10^{-5}	1.1×10^{-4}	8.1×10^{-6}	Model-dependent
m_ρ (GeV)	8.49×10^{6}	3.34×10^{7}	3.49×10^{8}	
η	$\sim 10^{-11}$	$\sim 10^{-11}$	$\sim 10^{-10}$	$(6.0 \pm 0.2) \times 10^{-10}$
$\lambda_H(M_{Pl})$	0.222	0.166	0.149	None
$\lambda_\sigma(M_{Pl})$	5.44×10^{-9}	4.5×10^{-7}	2.47×10^{-7}	
$\Delta\lambda_{HHH}$	-5%	-5%	-6%	$<1400\%$

This has implications for a general class of BSM theories that utilize complex singlet scalars and other new non-scalar fields. If the corrections from non-scalar contributions to SM triple Higgs and quartic couplings are tiny, any large correction to λ_{HHH} (such as a discrepancy from a SM value measured by the HL-LHC) would rule out such a class of theories, including SMASH. It will be up to the HL-LHC experiment to determine whether this is the case.

5. Conclusions

We have investigated suitable benchmark scenarios for the simplest SMASH model regarding the scalars and neutrinos, constraining the new Yukawa couplings and scalar couplings via the vacuum stability and theory perturbativity requirements. The model can easily account for the neutrino sector, predicting the correct light neutrino mass spectrum while evading the experimental bounds for right-handed heavy sterile Majorana neutrinos. In [58], the authors of the SMASH model performed a one-loop RGE analysis of the model and presented the two-loop RGE's. We have extended the analysis to two-loop to gain the increased precision needed for the combined achievement of a stabilized electroweak vacuum and a large-enough triple Higgs coupling correction to be sensitive at FCC-hh. To the best of the authors' knowledge, this is the first report on the connection between threshold correction to λ_H and one-loop correction to λ_{HHH}.

We found an interesting interplay between the triple Higgs coupling correction and the SM Higgs quartic coupling correction. A successful vacuum stabilization mechanism (threshold mechanism) in SMASH is consistent with small triple Higgs coupling corrections, requiring it to be at most $\sim 5\%$. Since the $\Delta\lambda_{HHH}$ is proportional to the threshold correction δ, a large correction to $\Delta\lambda_{HHH}$ inevitably leads to a large threshold correction. Detecting a λ_{HHH} correction larger than $\sim 35\%$ is within the sensitivity of a future high-luminosity upgrade of the LHC [40,41]. If detected, it would, therefore, rule out the simplest scalar sector of the model completely. This would force the model to develop non-minimal alternatives, such as an additional scalar doublet or triplet instead of a singlet. These alternatives were considered by the authors of the SMASH model in their recently updated study [60]. The lepton asymmetry $|\Delta L/\varepsilon_{CP}|$ is around 6×10^{-7} to 10^{-5} for the present-day scenario of the universe, which can be verified experimentally [83] at the FCC [47], LHC [84], and by the Circular Electron Positron Collider (CEPC) [85] for the SMASH framework.

Author Contributions: Conceptualization, C.R.D. and K.H.; methodology, T.J.K.; software, T.J.K.; validation, C.R.D. and T.J.K.; formal analysis, C.R.D. and K.H.; investigation, C.R.D.; resources, T.J.K.; data curation, T.J.K.; writing—original draft preparation, T.J.K.; writing—review and editing, C.R.D.; visualization, C.R.D.; supervision, K.H. All authors have read and agreed to the published version of the manuscript.

Notes

[1]   We integrate out ρ at the tree level and then compute loop corrections to the triple Higgs coupling in the resulting effective theory with ρ integrated out. By construction, the effective theory is just the SM plus higher-dimensional operators suppressed by inverse powers of m_ρ. Deviations from the SM triple Higgs coupling can then only come from the effects of the higher-dimensional operators, and so these deviations should involve the inverse powers of m_ρ which are in Equation (17). In other words, in the limit $m_\rho \to \infty$, one should recover the SM result, which Equation (17) does satisfy.

[2]   We acknowledge that neutrino Yukawa coupling matrix Y_ν should be complex in order to allow the leptogenesis scenario to work. The vacuum stability analysis, however, is unaffected by this, and we can safely ignore the imaginary parts of the Yukawa couplings in this part of the analysis.

[3]   https://pdg.lbl.gov/2022/reviews/rpp2022-rev-higgs-boson.pdf, page 29–30, chapter 11, Section 3.4.2 and page 66, chapter 11, Section 6.2.5.

References

1. Aad, G.; Abajyan, T.; Abbott, B.; Abdallah, J.; Khalek, S.A.; Abdelalim, A.A.; Aben, R.; Abi, B.; Abolins, M.; AbouZeid, O.S.; et al. Observation of a new particle in the search for the Standard Model Higgs boson with the ATLAS detector at the LHC. *Phys. Lett. B* **2012**, *716*, 1–29.
2. Chatrchyan, S.; Khachatryan, V.; Sirunyan, A.M.; Tumasyan, A.; Adam, W.; Aguilo, E.; Bergauer, T.; Dragicevic, M.; Erö, J.; Fabjan, C.; et al. Observation of a New Boson at a Mass of 125 GeV with the CMS Experiment at the LHC. *Phys. Lett. B* **2012**, *716*, 30–61.
3. Workman, R.L.; Burkert, V.D.; Crede, V.; Klempt, E.; Thoma, U.; Tiator, L.; Agashe, K.; Aielli, G.; Allanach, B.C.; Amsler, C.; et al. Review of Particle Physics. *PTEP* **2022**, *2022*, 083C01. [CrossRef]
4. Bass, S.D.; De Roeck, A.; Kado, M. The Higgs boson implications and prospects for future discoveries. *Nat. Rev. Phys.* **2021**, *3*, 608–624.
5. Alekhin, S.; Djouadi, A.; Moch, S. The top quark and Higgs boson masses and the stability of the electroweak vacuum. *Phys. Lett. B* **2012**, *716*, 214–219.
6. Nielsen, H.B.; Froggatt, C.D. Anomalies from Non-Perturbative Standard Model Effects. *arXiv* **2019**, arXiv:1905.00070.
7. Arbuzov, B.A.; Zaitsev, I.V. Calculation of the contribution to muon $g-2$ due to the effective anomalous three boson interaction and the new experimental result. *Int. J. Mod. Phys. A* **2021**, *36*, 2150223.
8. Arbuzov, B.A. The discrepancy in the muon $g-2$ is a non-perturbative effect of the Standard Model. *arXiv* **2013**, arXiv:1304.7090.
9. Wang, J.; Wen, X.G. Nonperturbative definition of the standard models. *Phys. Rev. Res.* **2020**, *2*, 023356.
10. Arbuzov, B.A. Non-perturbative Effective Interactions in the Standard Model. In *De Gruyter Studies in Mathematical Physics*; De Gruyter: Berlin, Germany; Boston, MA, USA, 2014; Volume 23. [CrossRef]
11. Bednyakov, A.V. An advanced precision analysis of the SM vacuum stability. *Phys. Part. Nucl.* **2017**, *48*, 698–703.
12. Abel, S.; Spannowsky, M. Observing the fate of the false vacuum with a quantum laboratory. *PRX Quantum* **2021**, *2*, 010349.
13. Markkanen, T.; Rajantie, A.; Stopyra, S. Cosmological Aspects of Higgs Vacuum Metastability. *Front. Astron. Space Sci.* **2018**, *5*, 40.
14. Lorenz, C.S.; Funcke, L.; Calabrese, E.; Hannestad, S. Time-varying neutrino mass from a supercooled phase transition: Current cosmological constraints and impact on the Ω_m-σ_8 plane. *Phys. Rev. D* **2019**, *99*, 023501.
15. Landim, R.G.; Abdalla, E. Metastable dark energy. *Phys. Lett. B* **2017**, *764*, 271–276.
16. Kohri, K.; Matsui, H. Electroweak Vacuum Instability and Renormalized Vacuum Field Fluctuations in Friedmann-Lemaitre-Robertson-Walker Background. *Phys. Rev. D* **2018**, *98*, 103521.
17. Masina, I. Higgs boson and top quark masses as tests of electroweak vacuum stability. *Phys. Rev. D* **2013**, *87*, 053001.
18. Fritzsch, H.; Gell-Mann, M.; Minkowski, P. Vecto—Like Weak Currents and New Elementary Fermions. *Phys. Lett. B* **1975**, *59*, 256–260. [CrossRef]
19. Minkowski, P. $\mu \to e\gamma$ at a Rate of One Out of 10^9 Muon Decays? *Phys. Lett. B* **1977**, *67*, 421–428. [CrossRef]
20. Gell-Mann, M.; Ramond, P.; Slansky, R. Complex Spinors and Unified Theories. *Conf. Proc. C* **1979**, *790927*, 315–321.
21. Yanagida, T. Horizontal Symmetry and Masses of Neutrinos. *Prog. Theor. Phys.* **1980**, *64*, 1103. [CrossRef]
22. Mohapatra, R.N.; Senjanovic, G. Neutrino Mass and Spontaneous Parity Nonconservation. *Phys. Rev. Lett.* **1980**, *44*, 912. [CrossRef]
23. Mohapatra, R.N.; Senjanovic, G. Neutrino Masses and Mixings in Gauge Models with Spontaneous Parity Violation. *Phys. Rev. D* **1981**, *23*, 165. [CrossRef]
24. Schechter, J.; Valle, J.W.F. Neutrino Masses in SU(2) × U(1) Theories. *Phys. Rev. D* **1980**, *22*, 2227. [CrossRef]
25. Magg, M.; Wetterich, C. Neutrino Mass Problem and Gauge Hierarchy. *Phys. Lett. B* **1980**, *94*, 61–64. [CrossRef]
26. Glashow, S.L. The Future of Elementary Particle Physics. *NATO Sci. Ser. B* **1980**, *61*, 687. [CrossRef]

27. Lazarides, G.; Shafi, Q. Neutrino Masses in SU(5). *Phys. Lett. B* **1981**, *99*, 113–116. [CrossRef]
28. Gelmini, G.B.; Roncadelli, M. Left-Handed Neutrino Mass Scale and Spontaneously Broken Lepton Number. *Phys. Lett. B* **1981**, *99*, 411–415. [CrossRef]
29. Bambhaniya, G.; Bhupal Dev, P.S.; Goswami, S.; Khan, S.; Rodejohann, W. Naturalness, Vacuum Stability and Leptogenesis in the Minimal Seesaw Model. *Phys. Rev. D* **2017**, *95*, 095016.
30. Abbott, L.F.; Sikivie, P. A Cosmological Bound on the Invisible Axion. *Phys. Lett. B* **1983**, *120*, 133–136. [CrossRef]
31. Preskill, J.; Wise, M.B.; Wilczek, F. Cosmology of the Invisible Axion. *Phys. Lett. B* **1983**, *120*, 127–132. [CrossRef]
32. Dine, M.; Fischler, W. The Not So Harmless Axion. *Phys. Lett. B* **1983**, *120*, 137–141. [CrossRef]
33. Bertolini, S.; Di Luzio, L.; Kolešová, H.; Malinský, M. Massive neutrinos and invisible axion minimally connected. *Phys. Rev. D* **2015**, *91*, 055014.
34. Salvio, A. A Simple Motivated Completion of the Standard Model below the Planck Scale: Axions and Right-Handed Neutrinos. *Phys. Lett. B* **2015**, *743*, 428–434.
35. Elias-Miro, J.; Espinosa, J.R.; Giudice, G.F.; Lee, H.M.; Strumia, A. Stabilization of the Electroweak Vacuum by a Scalar Threshold Effect. *J. High Energy Phys.* **2012**, *6*, 031.
36. Lebedev, O. On Stability of the Electroweak Vacuum and the Higgs Portal. *Eur. Phys. J. C* **2012**, *72*, 2058.
37. He, S.P.; Zhu, S.H. One-loop radiative correction to the triple Higgs coupling in the Higgs singlet model. *Phys. Lett. B* **2017**, *764*, 31–37; Erratum in *Phys. Lett. B* **2019**, *797*, 134782. [CrossRef]
38. Arhrib, A.; Benbrik, R.; El Falaki, J.; Jueid, A. Radiative corrections to the Triple Higgs Coupling in the Inert Higgs Doublet Model. *J. High Energy Phys.* **2015**, *12*, 007.
39. Arhrib, A.; Benbrik, R.; Chiang, C.W. Probing triple Higgs couplings of the Two Higgs Doublet Model at Linear Collider. *Phys. Rev. D* **2008**, *77*, 115013.
40. Cepeda, M.; Gori, S.; Ilten, P.; Kado, M.; Riva, F.; Abdul Khalek, R.; Aboubrahim, A.; Alimena, J.; Alioli, S.; Alves, A.; et al. Report from Working Group 2: Higgs Physics at the HL-LHC and HE-LHC. *CERN Yellow Rep. Monogr.* **2019**, *7*, 221–584.
41. Adhikary, A.; Banerjee, S.; Barman, R.K.; Bhattacherjee, B.; Niyogi, S. Higgs Self-Coupling at the HL-LHC and HE-LHC. *Springer Proc. Phys.* **2022**, *277*, 27–31. [CrossRef]
42. Arkani-Hamed, N.; Han, T.; Mangano, M.; Wang, L.T. Physics opportunities of a 100 TeV proton–proton collider. *Phys. Rept.* **2016**, *652*, 1–49.
43. Baglio, J.; Djouadi, A.; Quevillon, J. Prospects for Higgs physics at energies up to 100 TeV. *Rept. Prog. Phys.* **2016**, *79*, 116201.
44. Contino, R.; Curtin, D.; Katz, A.; Mangano, M.L.; Panico, G.; Ramsey-Musolf, M.J.; Zanderighi, G.; Anastasiou, C.; Astill, W.; Bambhaniya, G.; et al. Physics at a 100 TeV pp collider: Higgs and EW symmetry breaking studies. *arXiv* **2016**, arXiv:1606.09408.
45. Myers, S. The Future Circular Collider: Its potential and lessons learnt from the LEP and LHC experiments. *Res. Outreach* **2022**. [CrossRef]
46. Benedikt, M.; Blondel, A.; Janot, P.; Mangano, M.; Zimmermann, F. Future Circular Colliders succeeding the LHC. *Nat. Phys.* **2020**, *16*, 402–407. [CrossRef]
47. Blondel, A.; Janot, P. FCC-ee overview: New opportunities create new challenges. *Eur. Phys. J. Plus* **2022**, *137*, 92.
48. Myers, S. FCC: Building on the shoulders of giants. *Eur. Phys. J. Plus* **2021**, *136*, 1076. [CrossRef]
49. Aleksa, M.; Allport, P.P.; Asai, S.; Ball, A.; Besana, M.I.; Bielert, E.R.; Bologna, S.; Boos, E.; Borgonovi, L.; Bosley, R.; et al. Conceptual design of an experiment at the FCC-hh, a future 100 TeV hadron collider. *CERN Yellow Rep. Monogr.* **2022**, *2/2022*, 1–304. [CrossRef]
50. Baglio, J.; Weiland, C. Heavy neutrino impact on the triple Higgs coupling. *Phys. Rev. D* **2016**, *94*, 013002.
51. Baglio, J.; Weiland, C. Impact of heavy sterile neutrinos on the triple Higgs coupling. *PoS* **2017**, *EPS-HEP2017*, 143.
52. Baglio, J.; Weiland, C. The triple Higgs coupling: A new probe of low-scale seesaw models. *J. High Energy Phys.* **2017**, *4*, 038.
53. Dubinin, M.N.; Semenov, A.V. Triple and quartic interactions of Higgs bosons in the general two Higgs doublet model. *arXiv* **1998**, arXiv:hep-ph/9812246.
54. Dubinin, M.N.; Semenov, A.V. Triple and quartic interactions of Higgs bosons in the two Higgs doublet model with CP violation. *Eur. Phys. J. C* **2003**, *28*, 223–236.
55. Kanemura, S.; Kikuchi, M.; Yagyu, K. Radiative corrections to the Higgs boson couplings in the model with an additional real singlet scalar field. *Nucl. Phys. B* **2016**, *907*, 286–322.
56. Kanemura, S.; Kikuchi, M.; Yagyu, K. One-loop corrections to the Higgs self-couplings in the singlet extension. *Nucl. Phys. B* **2017**, *917*, 154–177.
57. Aoki, M.; Kanemura, S.; Kikuchi, M.; Yagyu, K. Radiative corrections to the Higgs boson couplings in the triplet model. *Phys. Rev. D* **2013**, *87*, 015012.
58. Ballesteros, G.; Redondo, J.; Ringwald, A.; Tamarit, C. Standard Model—Axion—Seesaw—Higgs portal inflation. Five problems of particle physics and cosmology solved in one stroke. *J. Cosmol. Astropart. Phys.* **2017**, *8*, 001.
59. Ballesteros, G.; Redondo, J.; Ringwald, A.; Tamarit, C. Unifying inflation with the axion, dark matter, baryogenesis and the seesaw mechanism. *Phys. Rev. Lett.* **2017**, *118*, 071802.
60. Ballesteros, G.; Redondo, J.; Ringwald, A.; Tamarit, C. Several Problems in Particle Physics and Cosmology Solved in One SMASH. *Front. Astron. Space Sci.* **2019**, *6*, 55.
61. Fukugita, M.; Yanagida, T. Baryogenesis Without Grand Unification. *Phys. Lett. B* **1986**, *174*, 45–47. [CrossRef]

62. Buchmuller, W.; Di Bari, P.; Plumacher, M. Cosmic microwave background, matter–antimatter asymmetry and neutrino masses. *Nucl. Phys. B* **2002**, *643*, 367–390; Erratum in *Nucl. Phys. B* **2008**, *793*, 362. [CrossRef]
63. Davidson, S.; Ibarra, A. A Lower bound on the right-handed neutrino mass from leptogenesis. *Phys. Lett. B* **2002**, *535*, 25–32.
64. Buchmuller, W.; Di Bari, P.; Plumacher, M. Leptogenesis for pedestrians. *Ann. Phys.* **2005**, *315*, 305–351.
65. Buchmüller, W. Leptogenesis: Theory and Neutrino Masses. *Nucl. Phys. B Proc. Suppl.* **2013**, *235–236*, 329–335.
66. Buchmüller, W. Leptogenesis. *Scholarpedia* **2014**, *9*, 11471. [CrossRef]
67. Esteban, I.; Gonzalez-Garcia, M.C.; Maltoni, M.; Schwetz, T.; Zhou, A. The fate of hints: Updated global analysis of three-flavor neutrino oscillations. *J. High Energy Phys.* **2020**, *9*, 178.
68. Aghanim, N.; Akrami, Y.; Ashdown, M.; Aumont, J.; Baccigalupi, C.; Ballardini, M.; Banday, A.J.; Barreiro, R.B.; Bartolo, N.; Basak, S.; et al. Planck 2018 results. VI. Cosmological parameters. *Astron. Astrophys.* **2020**, *641*, A6; Erratum in *Astron. Astrophys.* **2021**, *652*, C4. [CrossRef]
69. Goobar, A.; Hannestad, S.; Mortsell, E.; Tu, H. A new bound on the neutrino mass from the sdss baryon acoustic peak. *J. Cosmol. Astropart. Phys.* **2006**, *6*, 019.
70. Di Valentino, E.; Gariazzo, S.; Mena, O. Most constraining cosmological neutrino mass bounds. *Phys. Rev. D* **2021**, *104*, 083504.
71. Vagnozzi, S.; Giusarma, E.; Mena, O.; Freese, K.; Gerbino, M.; Ho, S.; Lattanzi, M. Unveiling ν secrets with cosmological data: Neutrino masses and mass hierarchy. *Phys. Rev. D* **2017**, *96*, 123503.
72. Hut, P.; Olive, K.A. A Cosmological Upper Limit on the Mass of Heavy Neutrinos. *Phys. Lett. B* **1979**, *87*, 144–146. [CrossRef]
73. Di Valentino, E.; Melchiorri, A. Neutrino Mass Bounds in the Era of Tension Cosmology. *Astrophys. J. Lett.* **2022**, *931*, L18.
74. Li, E.K.; Zhang, H.; Du, M.; Zhou, Z.H.; Xu, L. Probing the Neutrino Mass Hierarchy beyond ΛCDM Model. *J. Cosmol. Astropart. Phys.* **2018**, *8*, 042.
75. Naidoo, K.; Massara, E.; Lahav, O. Cosmology and neutrino mass with the minimum spanning tree. *Mon. Not. R. Astron. Soc.* **2022**, *513*, 3596–3609.
76. Mishra-Sharma, S.; Alonso, D.; Dunkley, J. Neutrino masses and beyond-ΛCDM cosmology with LSST and future CMB experiments. *Phys. Rev. D* **2018**, *97*, 123544.
77. Gariazzo, S. Neutrino Properties and the Cosmological Tensions in the ΛCDM Model. In Proceedings of the 15th Marcel Grossmann Meeting on Recent Developments in Theoretical and Experimental General Relativity, Astrophysics, and Relativistic Field Theories, Rome, Italy, 1–7 July 2018.
78. Zhao, M.M.; Li, Y.H.; Zhang, J.F.; Zhang, X. Constraining neutrino mass and extra relativistic degrees of freedom in dynamical dark energy models using Planck 2015 data in combination with low-redshift cosmological probes: Basic extensions to ΛCDM cosmology. *Mon. Not. R. Astron. Soc.* **2017**, *469*, 1713–1724.
79. Denton, P.B.; Friend, M.; Messier, M.D.; Tanaka, H.A.; Böser, S.; Coelho, J.a.A.B.; Perrin-Terrin, M.; Stuttard, T. Snowmass Neutrino Frontier: NF01 Topical Group Report on Three-Flavor Neutrino Oscillations. *arXiv* **2022**, arXiv:2212.00809.
80. Jegerlehner, F.; Kalmykov, M.Y.; Kniehl, B.A. On the difference between the pole and the $\overline{MS}$ masses of the top quark at the electroweak scale. *Phys. Lett. B* **2013**, *722*, 123–129.
81. Hamaguchi, K.; Murayama, H.; Yanagida, T. Leptogenesis from N dominated early universe. *Phys. Rev. D* **2002**, *65*, 043512.
82. He, H.J.; Ren, J.; Yao, W. Probing new physics of cubic Higgs boson interaction via Higgs pair production at hadron colliders. *Phys. Rev. D* **2016**, *93*, 015003.
83. Abdullahi, A.M.; Alzas, P.B.; Batell, B.; Boyarsky, A.; Carbajal, S.; Chatterjee, A.; Crespo-Anadon, J.I.; Deppisch, F.F.; De Roeck, A.; Drewes, M.; et al. The Present and Future Status of Heavy Neutral Leptons. In Proceedings of the 2022 Snowmass Summer Study, Seattle, WA, USA, 17–26 July 2022.
84. Alimena, J.; Beacham, J.; Borsato, M.; Cheng, Y.; Vidal, X.C.; Cottin, G.; Curtin, D.; De Roeck, A.; Desai, N.; Evans, J.A.; et al. Searching for long-lived particles beyond the Standard Model at the Large Hadron Collider. *J. Phys. G* **2020**, *47*, 090501.
85. Gao, J. Snowmass2021 White Paper AF3-CEPC. *arXiv* **2022**, arXiv:2203.09451.